Design and Analysis of a Magneto-Rheological Fluid Damper with Non-linear Surfaces to Produce Effective Variable Compliance in a Robotic Transmission

A Thesis

Presented in Partial Fulfillment of the

Requirements to Graduate 'with Distinction' at

The Ohio State University

By

Ehsan Sadeghipour

The Ohio State University

2009

Approved By: Examination Committee

Professor Marcelo Dapino _____

Professor Yann Guezennec _____

ABSTRACT

Our communities have been designed for human movement; therefore, the development of machines that locomote like humans is a natural approach to mechanical locomotion. Two problems in developing autonomous versions of these machines are energy consumption and the risks associated with the possible impact of robotic components with the humans around them. Research has shown that using variable compliance, or elasticity, in robotic joints can decrease both of these factors. This project is focused on the development of a variable compliance robotic transmission based on Magneto-Rheological (MR) fluid for increasing biped walking efficiency and decreasing the impact forces associated with a possible collision. The results of this study are important in developing autonomous robots that can safely interact with humans for an extended period of time.

This thesis is dedicated to Maman Jooni and Baba Jooni
for their infinite love, support, and emphasis on education.

ACKNOWLEDGEMENTS

I would like to thank my advisors Drs. Dapino, Schmiedeler, and Westervelt for their continued support throughout the years, and for giving me the opportunity to work with them.

TABLE OF CONTENTS

TABLE OF FIGURES

Chapter 1 INTRODUCTION

1.1 Objective

The objective of this study is to develop a method of numerically analyzing rotary Magneto-Rheological (MR) fluid dampers, and using this method to analyze a MR fluid damper with non-linear damping surfaces. Such a damper could then be put in parallel with a compliant element and controlled properly to produce effective variable compliance.

1.2 Motivation

As tens of millions of Baby Boomers retire in the coming years, attending to their medical needs will constitute one of the biggest challenges of American society. The issue of attending to aging populations is not unique to America as it already is an important issue in countries such as Japan and France. Autonomous biped robots that can safely function in our societies may be used to increase our quality of life and may be the key to serving aging populations around the world. Most of the physical components in our communities have been designed for human movement (i.e., stairs or curbs). Therefore, the development of machines that locomote like humans is a natural approach to mechanical locomotion. One of the greatest challenges in this process has been energy efficiency, which is important in the development of autonomous robots. For example Honda's ASIMO is currently one of the most advanced autonomous biped robots in the world, yet it has a battery life of only 25 minutes (Honda Motor Co. Ltd., 2007). One way of improving the energetic efficiency of a bipedal robot is to add compliance in the robot's transmission system. Further details of this phenomenon as well as the importance of variable compliance in the transmission system is provided in Section 1.3. In addition, new robots have

increasingly been designed with very stiff transmission systems in order to improve their accuracy and reduce the amount of time required for the acceleration or deceleration of the robotic component. While these systems meet the stated needs if contact between the robotic arm and a human occurs, the stiffness in their transmission can lead to injury of the human or it can damage the robot. Adding variable compliance to the robotic transmission system can ensure the effectiveness and accuracy of a robot as well as its safe operation. Further details of this phenomenon have been provided in Section 1.3.

Because of this need for variable compliance robotic transmission systems the Locomotion and Biomechanics Lab at The Ohio State University studied one way of producing such systems through several undergraduate and graduate projects. To produce such a device the lab placed a spring in parallel with an MR damper and controlled the system to produce robotic transmissions with effective variable compliance. Multiple students at that lab had worked on projects to improve the design of MR dampers used for such a purpose. This work was completed both on linear MR dampers and springs for linear robotic actuation systems, as well as on rotary MR dampers and torsion springs for rotary transmission systems. This research is a continuation of the effort to improve the effectiveness of these devices. As a part of this evolutionary process this project added protrusions to the damping surfaces of the device designed by a previous student. Further details of previous students' efforts are provided in Section 1.3.

1.3 Background

Low energetic efficiency is a major hurdle in the widespread adoption of bipedal robots as assistants in our society. Using springs in robotic transmission systems can be one way of

alleviating this problem. Alexander suggests increasing biped energy efficiency by using springs to store and then release energy in the cyclic up-and-down and back-and-forth leg movements inherent to walking and running (Alexander, 1990). The inspiration for these devices is based on their biological counterparts in humans and animals in the form of tendons and ligaments, which often act as springs to store mechanical energy. The ability of tendons and ligaments to act as springs is especially important in running, as running gaits are heavily dependent on the biped's (or quadruped's) ability to store and release bursts of mechanical energy in a short time period (McMahon, 1984). Yang et al. have shown that using compliance in parallel with the transmission at the knee joint reduces the energy use of the bipedal robot ERNIE (Yang, Westervelt, & Schmiedeler, 2007). They found that softer springs lead to greater efficiency of slow gaits, while stiffer springs lead to even greater efficiency of fast gaits. Therefore, in order for a bipedal robot to change the speed of its gait while maintaining high energetic efficiency, it must employ variable compliance in its transmission.

Many new robots have been designed with very stiff transmissions to improve the robotic arm's ability to accelerate or decelerate rapidly, and to allow for greater accuracy when the arm is reaching for an item. The drawback of stiff transmission systems is that contact between the robotic arm and a human or object in the vicinity can either injure the human or damage the robot. Bicchi et al. consider the importance of joint compliance in robotic transmissions to ensure the safety of the robot by reducing the impact forces of collision (Bicchi & Tonietti, 2004). They note that transmission compliance causes robotic joints to accelerate more slowly and decreases accuracy by increasing vibrations while decelerating. They propose the use of variable compliance in transmissions instead. The ability to vary transmission compliance allows for low

transmission compliance while accelerating, decelerating or at points in the arm's trajectory where a high level of accuracy is required. Yet transmission compliance may be increased at high speeds when the greatest chance of a dangerous collision exists.

Various methods have been suggested to produce variable compliance in robotic joints. Westervelt et al. show that by placing a MR fluid damper in parallel with a compliant element in an actuation system the effective compliance can be controlled to vary from highly compliant to essentially rigid (Westervelt, Schmiedeler, & Washington, 2004). When the damper is turned on the transmission is rigid, whereas when the device is turned off the transmission is highly compliant with low damping. The compliance range between the two extremes is realized through control algorithms that include switching. This behavior is achieved by exploiting the properties of the MR fluid in the damper.

The force required to deform an elastic solid is proportional to the amount of deformation, with the proportionality constant being the elastic modulus of the material. However, to better understand how effective variable compliance may be achieved using a variable damper in parallel with a compliant element such as a spring one must consider a viscoelastic model instead. Figure 1.1 presents the visual model for a viscoelastic material.

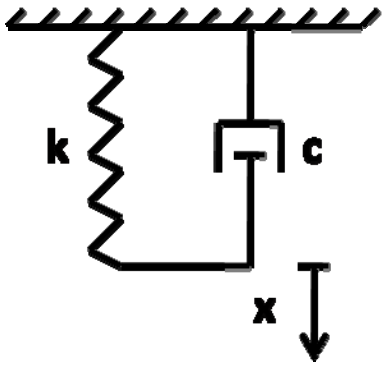

Figure 1.1: Model of a Viscoelastic Material

Equation 1.1 presents the mathematical model of a viscoelastic material in Laplace domain. This mathematical model corresponds to the visual model presented in Figure 1.1. This model refers to the stiffness of the material, which is inversely related to the compliance of that material.

1.1

$$F_{el}(s) = k_{eff}(s) \cdot X(s) \rightarrow k_{eff}(s) = k + cs$$

F_{el} = *Force Required to Elongate Material*
k_{eff} = *Effective Stiffness of Viscoelastic Material*
X = *Elongation of Viscoelastic Material*
k = *Component ofStiffness Related to Position (Elasticity)*
c = *Component of Stiffness Related to Velocity (Damping)*

The effective stiffness of a viscoelastic material is not only a function of the amount of elongation of that material, but also it is a function of the rate at which this elongation is taking place. The effective stiffness of a variable compliance robotic transmission may similarly be changed using an MR damper. In such a case, the amount of damping provided by the damper is varied to obtain an effective variable compliance.

Bunting developed an experimental apparatus and control algorithm for developing variable compliance in a rotary robotic transmission system (Bunting, 2005). Bunting's setup used a commercially available MR disk clutch (model MRB-2107-3) designed and manufactured by Lord Corporation. Preliminary testing, however, showed that this device exhibited a significant amount of backlash that made it difficult to properly and accurately position the device. This problem led to the development of a new MR disk clutch that avoided such a backlash, and one that could be used within the experimental apparatus already designed and built by Bunting.

Sabatka designed and built a new MR disk clutch for this experiment. Savatka's device was designed in a way to avoid the backlash present in Bunting's commercially acquired device, and it was dimensioned so that it could be used in the experimental setup created by Bunting (Sabatka, 2006). Sabatka's device used a steel shaft, piston, and cylinder, 1210 rounds of wire in its coil, and an MR foam to contain the MR fluid in the device. MR foam was useful in avoiding one of the main shortcomings of MR dampers, which is the leakage of the MR liquid. However, the foam has been designed in a way to avoid any interference with the fluid shearing process to such a point that it does not need to be accounted for when modeling the behavior of the device.

The two most important variables in this study are the size of the gap between the piston and the cylinder and the magnetic flux density within the MR fluid. A small gap results in a greater magnetic flux density within the fluid and a higher on-state holding torque; however, such a design choice also increases the off-state damping coefficient, which is undesirable. The opposite of these conditions is true for a large gap. The non-linear nature of magnetic flux may be used to overcome this inverse relationship between gap size and off-state damping. As an analogy, one

may consider the magnetic flux lines between two parallel plates, which are almost straight lines; however, a protrusion on one of the plates causes the flux lines in that area to congregate around the protrusion and fringe flux lines will emanate from the sides of the protrusion. Therefore, for the same average gap between two sets of parallel plates, the set with the protrusions will produce a greater amount of magnetic flux density in the gap.

The novel approach of this project is to apply this principle to the MR damper. This project modified the design created by Sabatka by adding rectangular non-linearities along the circumference of the piston surface while keeping the average gap the same as the simple case studied by Sabatka. This setup should allow for an increase in the range of damping possible using this device as the non-linearities will increase the maximum magnetic flux density possible in the gap. Keeping the average gap constant will allow for the lower end of the damping coefficient to remain roughly the same. This project is focused on studying the effects of these non-linearities on the behavior of the device, and whether an increase in the bandwidth of the system is possible when using them.

Chapter 2 METHODOLOGY

2.1 MR Fluid

A Newtonian fluid is one that strains continuously when a shear stress is applied to it, and the applied shear stress is linearly related to the strain rate. This linear relationship is called viscosity. Inactivated MR fluid (no magnetic field acts on the fluid) essentially behaves Newtonian, and it has a viscosity equal to that of its base fluid, which is usually a hydrocarbon-based fluid. Activated MR fluid (a magnetic field acts on the fluid) is not a Newtonian fluid because of two reasons: (i) at very high shear rates the fluid exhibits a shear-thinning behavior (e.g., the fluid behaves less viscous at higher shear rates than at lower shear rates) (Farjoud, Vahdati, & Fook Fah, 2008); (ii) activated MR fluid does not strain continuously under shear stress, and a minimum or yield shear stress must be applied to it before it begins to strain (Dapino, 2008).

The damper designed for this study is not operated at very high frequencies; therefore, the shear thinning effects mentioned are negligible and need not be included in the model. It is emphasized that the yield stress associated with an activated MR fluid depends on the magnetic flux density through the fluid. The yield stress increases as the magnetic flux density through the fluid is increased, and the yield stress decreases as the magnetic flux density is lowered. As a matter of fact, the designation of MR fluid as a "Smart Material" with dynamic material properties is because of this change in the yield stress of the activated fluid.MR fluid exhibits these properties because it contains micron-sized ferrous particles, usually iron, that align to increase the apparent

viscosity of the fluid when placed in a magnetic field. Higher magnetic flux densities lead to greater alignment of these particles, which in turn increases fluid viscosity. Certain chemicals are added to the base fluid to avoid the sedimentation of these particles. The small size of these particles allows them to align quickly, which gives MR fluid a rapid response time (on the order of milliseconds). This short response time is very beneficial for effective control of a system containing this fluid.

Knowledge of the physical principles that lead to the behavior of MR fluid allows us to better understand two more properties of this material: saturation and hysteresis. Greater magnetic flux densities lead to a greater alignment of the ferrous particles in the fluid, which leads to a greater viscosity. However, one can imagine how gradually increasing levels of magnetic flux density will be required to produce the same increase in the level of particle alignment. In addition, one can also imagine how there will be a limit to this alignment and after some point increasing levels of magnetic flux density will not lead to any increase in the fluid's viscosity. Furthermore, the magnetic characteristics of these particles mean that after alignment, some extra effort must be exerted to return these particles to their original position. This extra effort makes MR fluid a hysteretic material.

2.2 MR Fluid Model

These material behaviors are also evident in the equations used to mathematically model this material. As previously noted inactivated MR fluid acts like a Newtonian fluid; therefore, its behavior may be modeled using Equation 2.1.

2.1

$$\tau = \mu \cdot \dot{\gamma}$$

τ = *Shear Stress Applied* (Pa)
μ = *Fluid Viscosity* $(Pa \cdot s)$
$\dot{\gamma}$ = *Shear Rate* (s^{-1})

However, this model cannot be used for an activated MR fluid because it does not capture the fact that a yield, or minimum, stress is required before an activated MR fluid begins to strain. The activated MR fluid may be modeled as a Bingham fluid instead. The mathematical model of a Bingham fluid has been presented as Equation 2.2.

2.2

$$\tau = \tau_y(B) + \mu \cdot \dot{\gamma}$$

τ = *Shear Stress Applied* (Pa)
τ_y = *Yield Shear Stress* (Pa)
μ = *Fluid Viscosity* $(Pa \cdot s)$
$\dot{\gamma}$ = *Shear Rate* (s^{-1})
B = *Magnetic Flux Density* (T)

The yield stress is a function of the magnetic flux density in the MR fluid. Further details of the relationship between the yield stress and the magnetic flux density will be provided in later sections. Figure 2.1 presents a graphical representation of this phenomenon. The first solid line represents the model of a Newtonian or inactivated MR fluid, the second solid line represents the model of an activated MR fluid, and the dashed line represents the effective viscosity of the activated MR fluid at a particular shear rate.

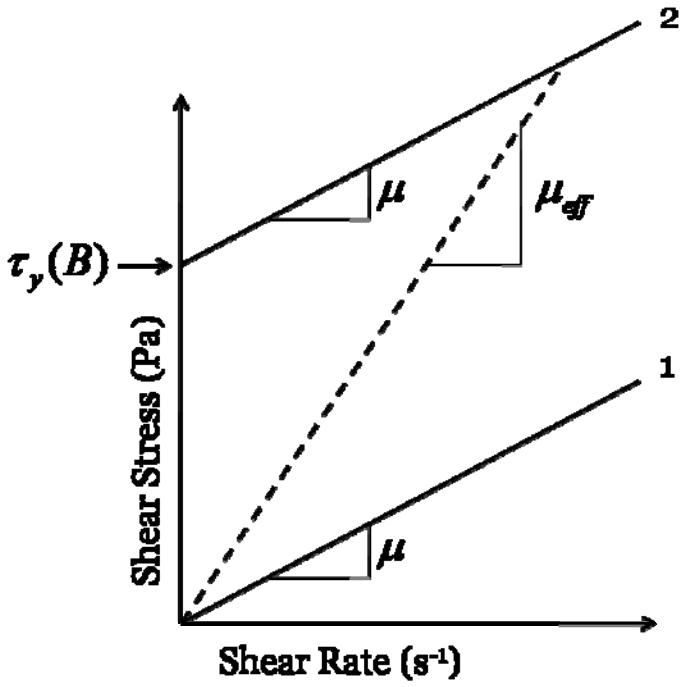

Figure 2.1: Activated MR Fluid and Yield Stress

Using the concept of effective viscosity, the behavior of MR fluid may be mathematically formulated through Equation 2.3.

2.3

$$\tau = \mu_{eff} \cdot \dot{\gamma}$$

μ_{eff} = *Effective Activated MR Fluid Viscosity* $(Pa \cdot s)$

The effective viscosity is dependent on the yield stress and shear rate, and it has been mathematically formulated in Equation 2.4.

2.4

$$\mu_{eff} \cdot \dot{\gamma} = \tau_y(B) + \mu \cdot \dot{\gamma} \rightarrow \mu_{eff} = \frac{\tau_y(B)}{\dot{\gamma}} + \mu$$

Understanding the issue of effective viscosity is important in understanding the behavior of the activated MR fluid. The effective viscosity means that for each combination of yield stress and

shear rate the activated MR fluid will behave similar to a Newtonian fluid with a viscosity equal to the effective viscosity of the MR fluid. Therefore, one way to ease the modeling of this material will be to specify the yield stress and shear rate, and use the effective viscosity model to treat the material like a Newtonian fluid. Treating the activated MR fluid as a Newtonian fluid allows one to take advantage of the various analytical solutions that exist for devices that incorporate Newtonian fluids.

2.3 Device

The MR damper designed was a rotary damper based on the design created by Kyle Sabatka. The decision to follow that design was based on the expectation that if a prototype of the new design was produced the experimental setup of Bunting could be used to test the new device.

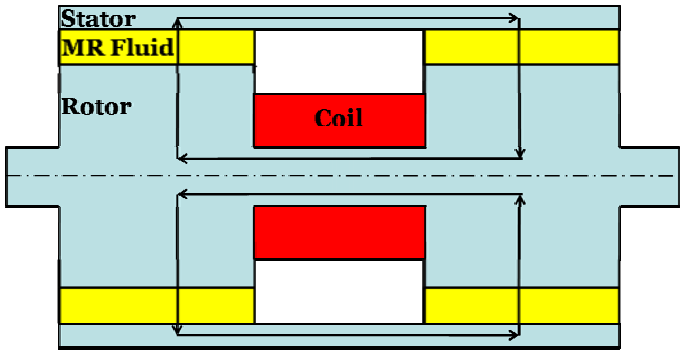

Figure 2.2: Side Cross-sectional View of Rotary Damper

Figure 2.2 presents the side cross-sectional view of a general rotary damper. The arrows in this figure represent the path of the magnetic flux lines based on the position of the coil, the rotor, and the stator. The magnetic flux lines travel perpendicular to the surface of the rotor, through the MR fluid, through the stator, back through the MR fluid, and finally complete the circuit in

the rotor. Figure 2.3 presents a more detailed cross-sectional and side view of one of the two piston sections of the classic damper designed by Sabatka. The radius of the piston in this model is 34.9 mm, the length of each piston section is 9.1 mm, the inside radius of the cylinder is 37.9 mm, and the outside radius of the cylinder is 42.7 mm. Figure 2.4 presents a more detailed cross-sectional and side view of one of the two piston sections of the non-linear damper designed for this study. The radius and length of the piston as well as the outside radius of the cylinder in this model have remained the same. The inside radius of the cylinder has been increased to 38.2 mm, while small rectangular protrusions with a height of 0.80 mm and a width of 0.76 mm have been added at even intervals to the circumference of that surface. The average gap of the non-linear model has remained the same as the gap in the classic model developed by Sabatka.

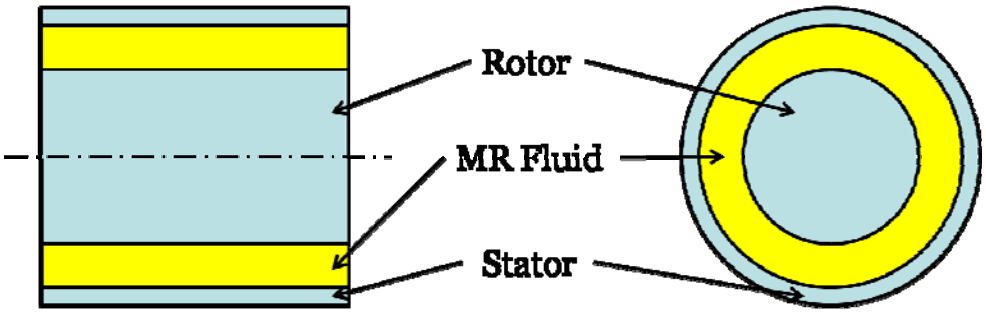

Figure 2.3: Cross-sectional and Side Views of Classic Damper

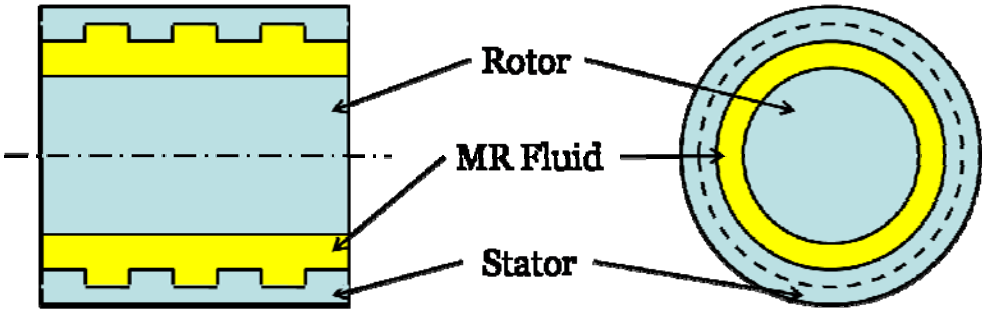

Figure 2.4: Cross-sectional and Side Views of Non-linear Damper

The viscosity of the MR fluid depends on the Magnetic flux density *B*, which is measured in Tesla, and is defined as the amount of magnetic flux through a particular surface area. This relationship has been presented in Equation 2.5. Note that this equation assumes that the surface area through which magnetic flux lines travel is constant, but in this case that area increases. Furthermore, it assumes that the flux density throughout the area is a constant, whereas one must integrate magnetic flux over the entire surface to obtain the correct value.

2.5

$$B = \frac{\varphi}{A_{S\_P}}$$

B = *Magnetic Flux Density* (T)
φ = *Magnetic Flux* (Wb)
A_{S_P} = *Surface Area of Piston* (m^2)

The relationship for the surface area of the piston has been presented in Equation 2.6.

2.6

$$A_{S\_P} = \pi \cdot D_P \cdot L_P$$

D_P = *Piston Diameter* (m)
L_P = *Piston Length* (m)

The expression for the magnetic flux has been presented as Equation 2.7.

2.7

$$\varphi = \frac{N \cdot I}{R}$$

N = *Number of Coil Turns* $(Turns)$
I = *Current through Coil* (A)
R = *Magnetic Reluctance* $\left(\frac{A \cdot Turns}{Wb}\right)$ → *Resistance of Magnetic Circuit*

The magnetic reluctance defined in Equation 2.7 is a function of the structure of the damper and the materials used in the damper, and it cannot be changed after the device has been built. In addition, the coil turns in the device are also difficult to change after the damper has been built. Therefore, based on Equations 2.5 and 2.7 the only realistic way to change the magnetic flux density, thus the viscosity of the MR fluid, is to change the current through the coil.

2.4 Analysis

The manufacturer of the MR fluid provides information about the relationship of the yield stress of that fluid and the magnetic flux density in the fluid. Figure 2.5 presents the typical magnetic properties of MRF-122EG MR fluid (courtesy of Lord Corporation). Figure 2.6 presents the yield stress versus the magnetic field strength of MRF-122EG MR fluid (courtesy of Lord Corporation). Figure 2.7 presents the shear stress versus shear rate for the MRF-122 MR fluid with no magnetic field applied (courtesy of Lord Corporation).

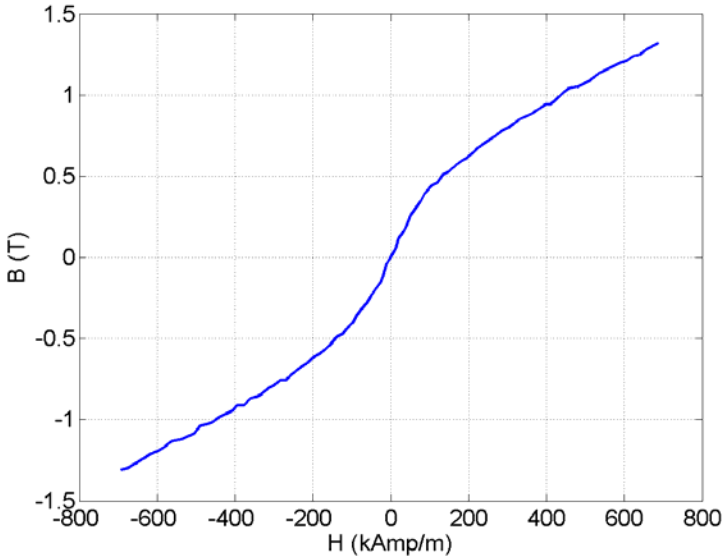

Figure 2.5: Magnetic Properties of MR Fluid (Courtesy of Lord Corp)

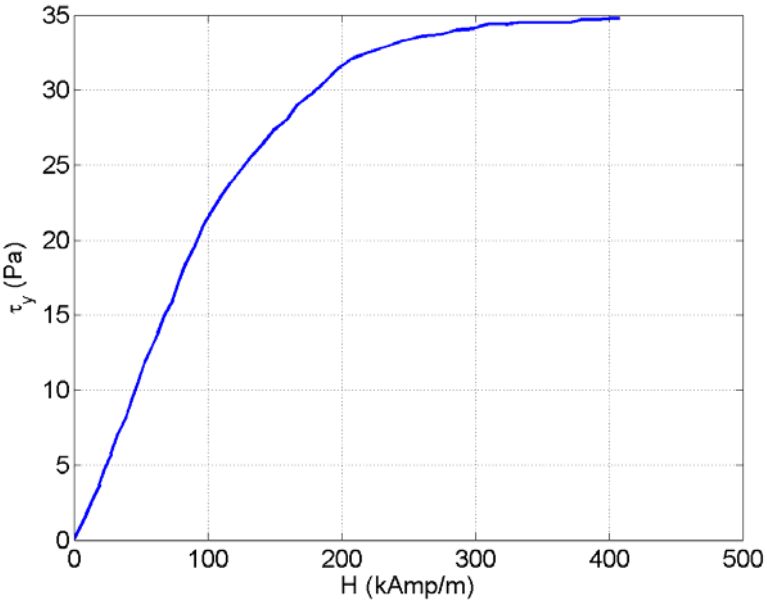

Figure 2.6: Yield Stress vs. Magnetic Field Strength of MR Fluid (Courtesy of Lord Corp)

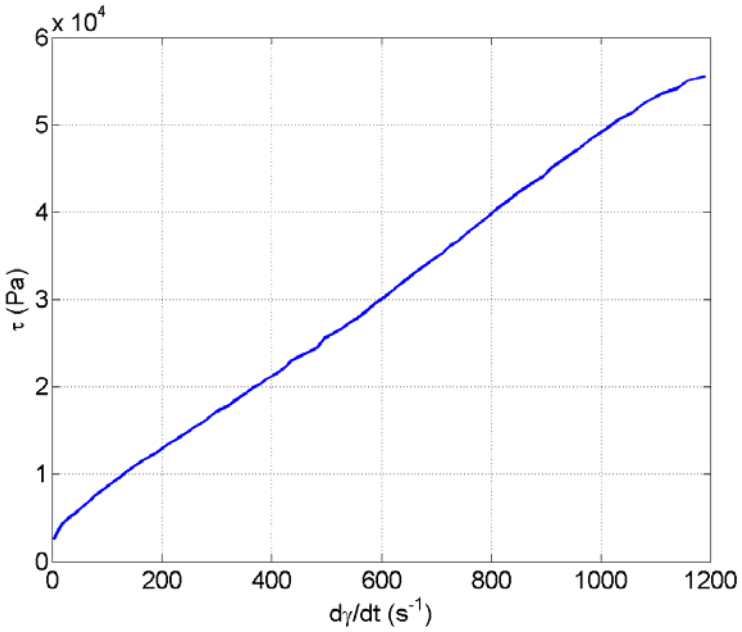

Figure 2.7: Shear Stress vs. Shear Rate of Inactivated MR Fluid (Courtesy of Lord Corp)

Using the data provided by the manufacturer, Equation 2.5, and Equation 2.7 one can relate the yield stress of the activated MR fluid to the current in the coil. This fact means that the only input required in calculating the yield stress component of Equation 2.2 is the current through the damper coil. The second term in Equation 2.2 is dependent on the viscosity of the inactivated MR fluid, which is a constant, and the shear rate of the fluid, which is related to the angular velocity of the device. In other words, based on the Bingham model of the activated MR fluid, the total shear stress on the damper wall has two components, and each component is a function of a single input. Having realized this fact, one can decouple this model into a magnetic component dependent on the current through the coil, and a fluid component dependent on the angular velocity of the rotor. This decoupling of the problem into a magnetic and a fluid component allows each part to be modeled in a separate numerical analysis program. Equation 2.8 presents the decoupled view of the Bingham model for the activated MR fluid.

2.8

$$\tau_T(I,\omega) = \tau_M(B) + \tau_F(\dot{\gamma}) = \tau_M(I) + \tau_F(\omega)$$

τ_T – *Total Shear Stress* (*Pa*)
τ_M – *Magnetic Component of Shear Stress* (*Pa*)
τ_F – *Fluid Component of Shear Stress* (*Pa*)
I – *Current through the Coil* (*A*)
ω – *Angular Velocity of Rotor* (*rpm*)

Based on Equation 2.8 the device was analyzed using two different Finite Element Analysis (FEA) programs. The freeware program Finite Element Method Magnetics (FEMM) was used to analyze the magnetic component. To allow for repeatability of the analysis the OctaveFEMM component of FEMM was used. Instead of the Graphic User Interface (GUI) provided by FEMM, OctaveFEMM provides a text-based interface through the MATLAB computer program. The analysis of the fluid component was achieved through the FLOTRAN component of the

ANSYS FEA program. The text-based interface of ANSYS instead of the GUI interface was used to allow for repeatability of the analysis of the fluid component.

Adding these two components yields the total shear stress. The total shear stress at the piston wall can then be multiplied by the surface area and radius of the piston to calculate the maximum torque produced by the device at a particular coil current and angular velocity. The expression for this torque has been presented as Equation 2.9.

2.9

$$T = \tau_T \cdot (2 \cdot A_{S-P}) \cdot \frac{D_P}{2} = \tau_T \cdot \pi \cdot D_P^2 \cdot L_P$$

As seen in Equation 2.9 the torque produced by the damper is a function of the shear stress on the surface of the piston, the radius of the piston, and the length of the piston. Please note that the surface area of the piston has been doubled to account for the fact that two separate surface areas of the piston come into contact with the MR fluid, and the fluid exerts a shear stress on each one.

2.5 OctaveFEMM Model

Chapter 3 The magnetic component of this decoupled problem was analyzed in OctaveFEMM. Figure 2.8 presents the OctaveFEMM model of the classic case rotary MR damper, and Figure 2.9 presents the OctaveFEMM model of the MR damper with non-linear surfaces. CONCLUSIONS

Designing robotic joints with effective variable compliance is an important technology in developing autonomous, safe, and energetically efficient robots. Effective variable compliance may be produced by putting a compliant element such as a spring in parallel with a variable damper such as an MR damper. Effective variable compliance is then achieved through the proper control of this mechanism, which will include switching. Because of this principle many students at OSU's Locomotion and Biomechanics Lab worked to develop linear and rotary MR dampers to be used in robotic transmissions with effective variable compliance. This project studied the effect of adding non-linearities to the inside surface of the cylinder in these dampers in order to increase the magnetic flux density in the fluid gap, while keeping the average fluid gap constant. Such a change was intended to increase the bandwidth of these devices.

This problem was decoupled into a magnetic component and a fluid component. The magnetic component was numerically analyzed in the FEA environment of OctaveFEMM, and the fluid component was analyzed using in the FLOTRAN environment of the computer code ANSYS. Using this setup the magnetic flux density in the gap increased by 21.9%, while the shear stress on the piston wall increased by 10.1%. These results suggest that adding non-linearities to the inside surface of the cylinder while maintaining the same average gap leads to a greater increase in the magnetic flux density in the gap than it does in the shear stress on the piston surface. This fact should allow for the design and development of effective variable compliance robotic transmissions with a greater bandwidth. Such a development in turn will allow for safer and more energetically efficient autonomous robots.

There are further steps that may be taken in improving this analysis. This problem was decoupled into magnetic and fluid components to simplify the analysis; however, by avoiding this

decoupling a more accurate study may be possible. Computer programs such as COMSOL allow for the fluid and magnetic components to be analyzed simultaneously, which will avoid the decoupling of this problem. Furthermore, a full analysis of the effect of non-linearities on the performance of this device must include an experimental component to compare the classic MR damper to the non-linear version. In addition, instead of rectangular non-linearities other studies could add semi-circular, triangular, or trapezoidal non-linearities as well. Finally, the effect of damper size on the behavior of the damper may be analyzed by designing multiple classic and non-linear MR dampers with varying overall dimensions but constant relative dimensions. This future work will be important in more conclusively determining the effect of non-linearities on the behavior of MR dampers.

APPENDIX A includes the code used to create these two models. Both designs are axis-symmetric cylinders; therefore, they have been modeled as axis-symmetric devices in a two

dimensional R-Z cylindrical coordinate system. Table 3.1 presents the material properties used for this magnetic circuit. The relative permeability presented in this table is essentially a measure of a particular material's ability to conduct magnetic flux lines, and it is inversely related to the magnetic reluctance variable defined earlier.

Table 3.1: Material Properties of Components

Material	Component	Relative Permeability (Unitless)
Air	Air	1
Aluminum	Outside Flanges	1
Copper	Coil	1
MR Fluid	MR Fluid	3.5
Steel	Rotor, Stator, Shaft	2000

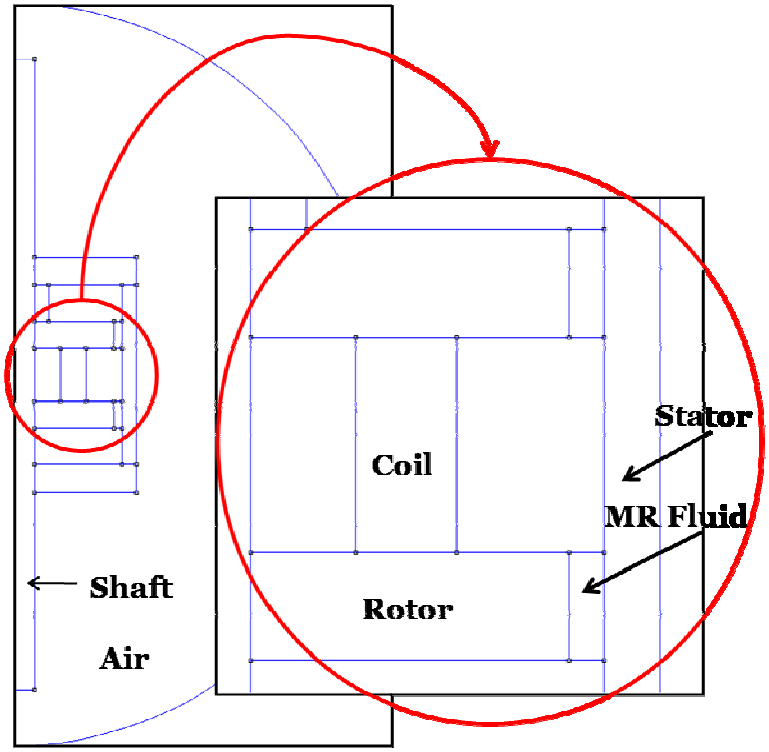

Figure 3.1: OctaveFEMM Model of the Classic Case MR Damper

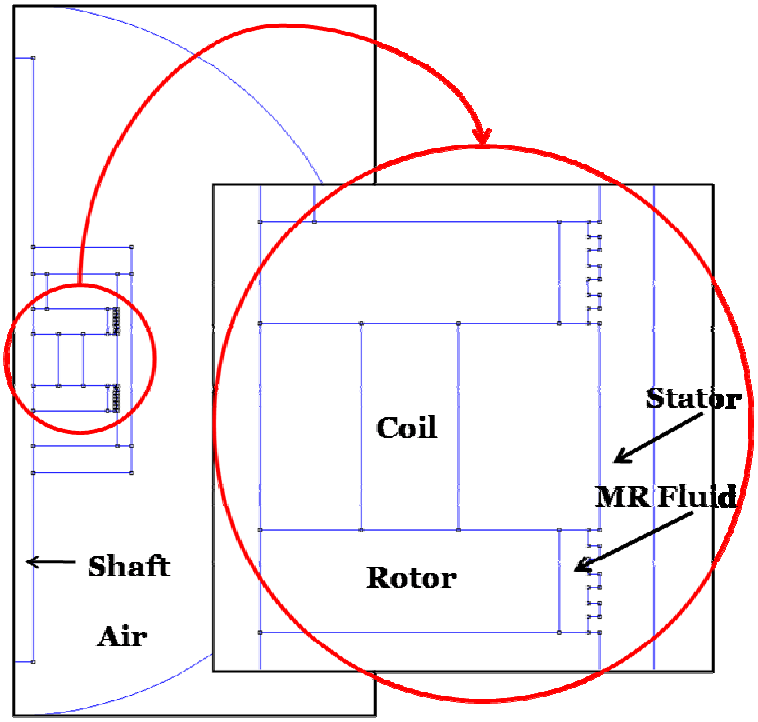

Figure 3.2: OctaveFEMM Model of MR Damper with Rectangular Cutouts

The line of symmetry in this model was given axis-symmetric boundary properties, and the semicircle around the device was modeled as a series of points so far away from the device that the magnetic field at those points is zero. Based on Sabatka's device the coil region was modeled with 1210 rounds of copper wire.

2.6 ANSYS Model

The fluid component of this device was modeled in the FLOTRAN environment of the computer code ANSYS. The fluid component of a classic case MR damper may simply be defined as a cylindrical Couette flow problem, which can be solved analytically. However, the FLOTRAN program is required in solving the non-linear case. Example 46 of the ANSYS Verification Manual (VM46.dat) solves a Couette flow problem presented on page 110 of Frank White's

Viscous Fluid Flow (White, 2005). This example was modified to fit the classic case damper model, and it was further modified to match the non-linear damper model. Figure 3.10 presents the isometric view of the ANSYS model of the classic case rotary MR damper, and Figure 3.11 presents the top view of this model. Figure 3.12 presents the isometric view of the ANSYS model of the MR damper with non-linear surfaces, and Figure 3.13 presents the top view of this model. APPENDIX B includes the code used to create these two models.

The fluid component in each case is simply a ring of fluid, which may be modeled as a series of fluid "wedges" that appear with periodicity to form the entire ring. Modeling the ring as a series of wedges is possible because of the periodicity of the fluid flow pattern, and it allows the problem to be solved much faster in ANSYS even with a relatively fine mesh. Based on this principle wedges with a thickness of only 10 degrees out of the 360 degrees of the ring were created in ANSYS. Based on the data provided by the MR fluid manufacturer the viscosity of the fluid model was set to 0.042 Pa-s and the density of the fluid model was set to 2380 Kg/m^3. The top and bottom surfaces of the wedges in Figure 3.10 and Figure 3.12 have been given periodic boundary conditions. The front and back surfaces in these figures have been given symmetry boundary conditions, which means that they extend infinitely long. The output of interest for this program is wall shear stress, which is defined as force per surface area, and will not be affected by how long the model is. The right surface, which comes into contact with the cylinder, was given the boundary condition of a moving wall with a velocity of zero in all directions. The left surface, which comes into contact with the piston, was given the boundary condition of a moving wall with a velocity of zero in all directions except one. In the θ direction the surface was give a velocity equal to the product of the piston radius and the angular velocity.

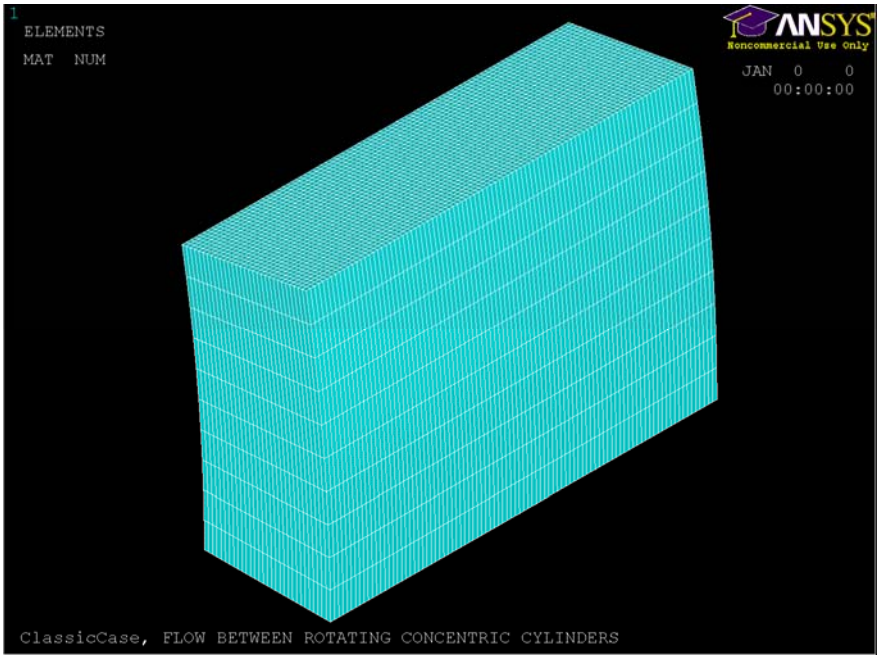

Figure 3.3: Isometric View of ANSYS Model of MR Damper (Classic Case)

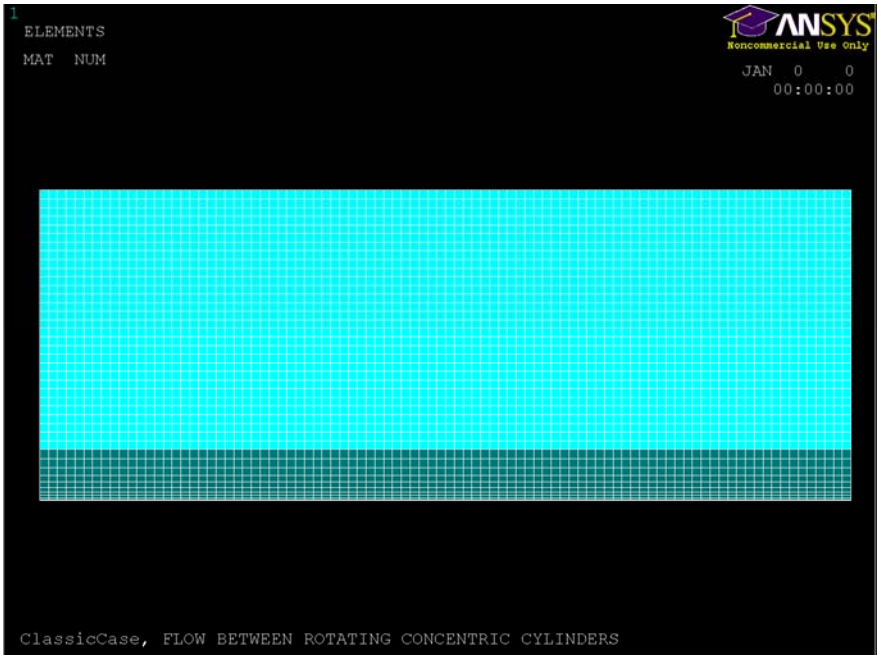

Figure 3.4: Top View of ANSYS Model of MR Damper (Classic Case)

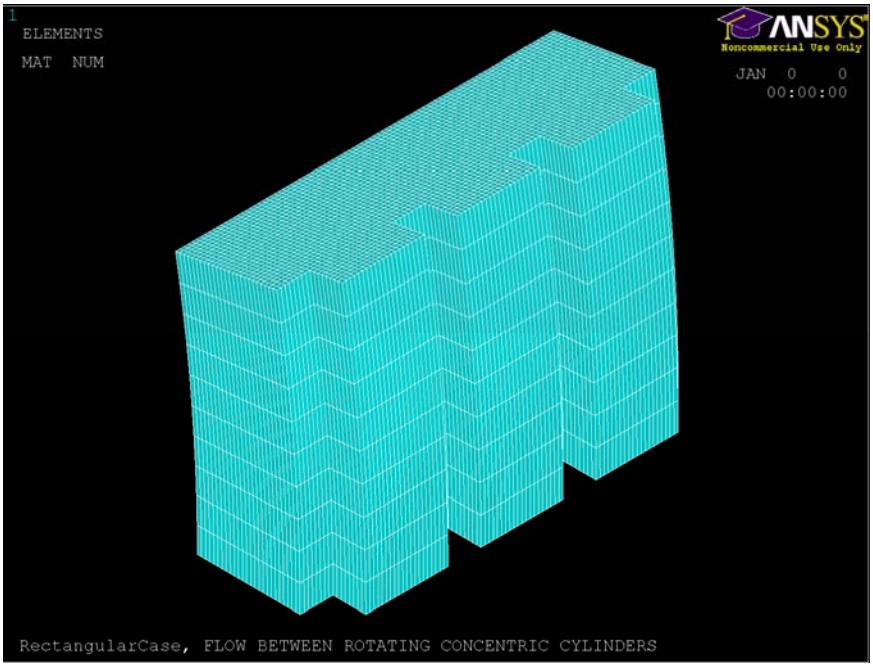

Figure 3.5: Isometric View of ANSYS Model of MR Damper (Non-linear Case)

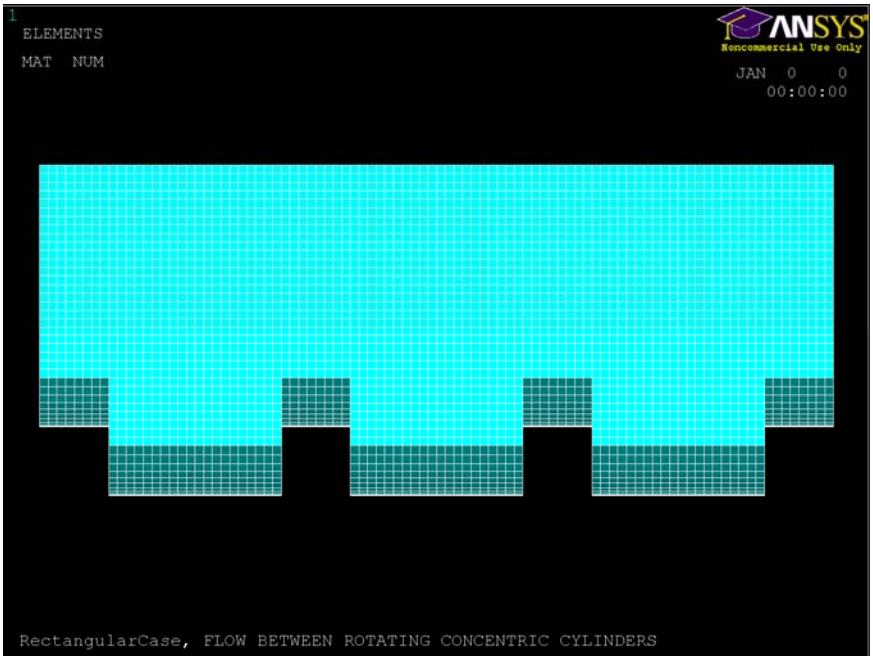

Figure 3.6: Top View of ANSYS Model of MR Damper (Non-linear Case)

Chapter 4 RESULTS

3.1 OctaveFEMM Results

Figure 4.1 presents the output of OctaveFEMM for the classic case damper model. Figure 4.2 presents the output of OctaveFEMM for the non-linear case damper model. Since OctaveFEMM is run through MATLAB the magnetic flux density throughout the MR fluid for each model can be calculated and averaged. The average magnetic flux density within the MR fluid in the classic case MR fluid damper is 0.825 T, and the average magnetic flux density within the MR fluid in the non-linear case MR fluid damper is 1.006 T. These results were obtained for a coil with 1210 rounds of wire, an electric current of 1.0 Amp, and different results should be expected for a different coil size or electric current. Therefore, the design change represents an increase of 21.9% in the magnetic flux density within the MR fluid.

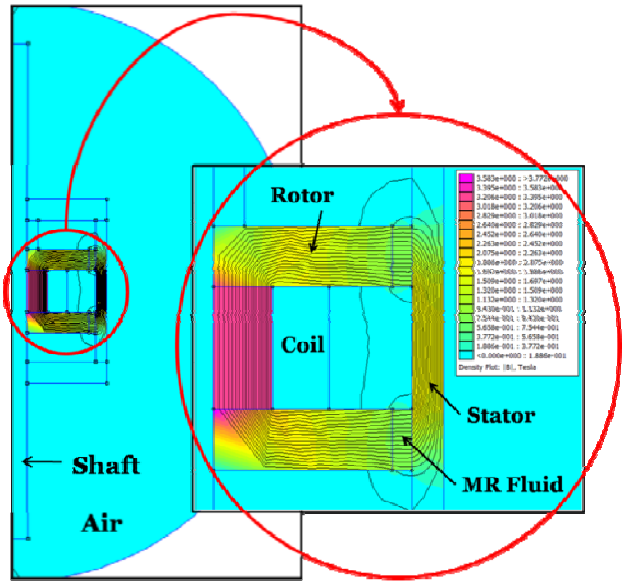

Figure 4.1: OctaveFEMM Results for the Classic Case MR Damper

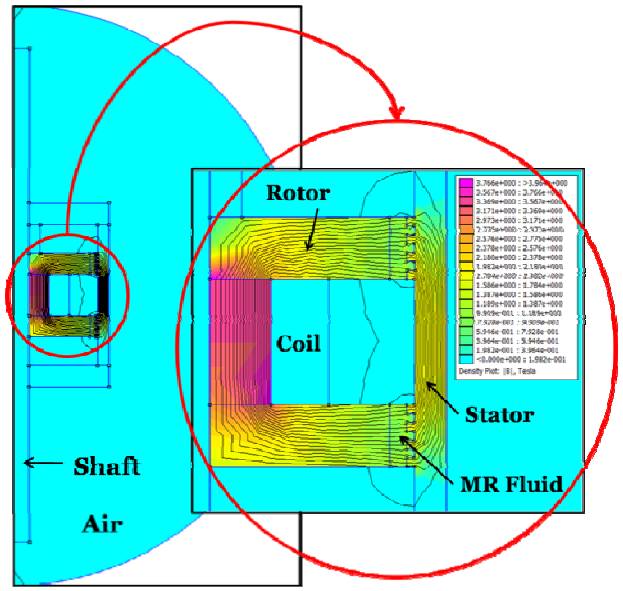

Figure 4.2: OctaveFEMM Results for the non-linear case MR Damper

3.2 ANSYS Results

Figure 4.3 presents an isometric view of the fluid velocity profile for the classic damper. Figure 4.4 presents a top view of the fluid velocity profile for the classic damper. Figure 4.5 presents an isometric view of the shear stress profile for the classic damper. Figure 4.6 presents the shear stress profile on the piston of the classic damper. Figure 4.7 presents isometric view of the fluid velocity profile for the non-linear damper. Figure 4.8 presents a top view of the fluid velocity profile for the non-linear damper. Figure 4.9 presents an isometric view of the shear stress profile for the non-linear damper. Figure 4.10 presents the shear stress profile on the piston of the non-linear damper. The average shear stress on the piston for the classic damper was 55.4 Pa, and the average shear stress on the piston for the non-linear damper was 61.0 Pa. In other words this design change led to an increase of 10.1% in the off-state damping of the MR Fluid damper. These results were obtained for an angular velocity of 100 rad/s or 955 rpm, and they will be different for other values of angular velocity.

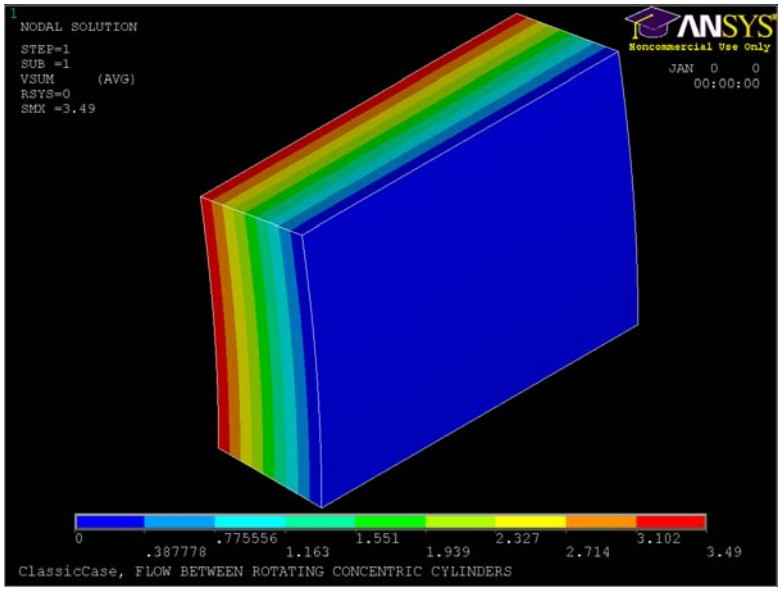

Figure 4.3: Isometric View of Velocity Profile (Classic Case)

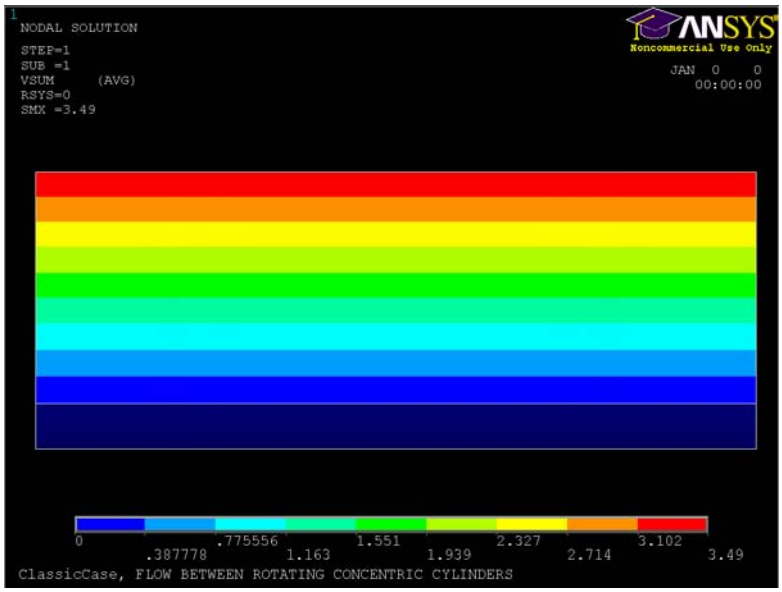

Figure 4.4: Top View of Velocity Profile (Classic Case)

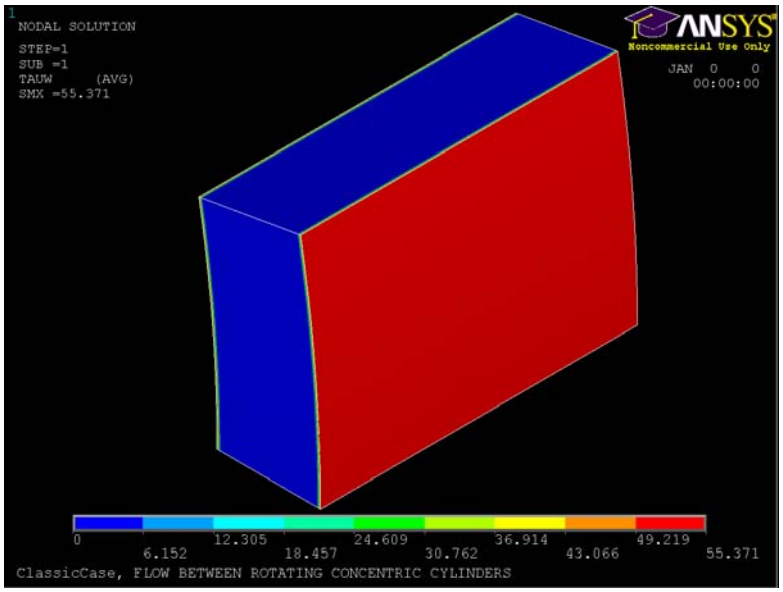

Figure 4.5: Isometric View of Shear Stress Profile (Classic Case)

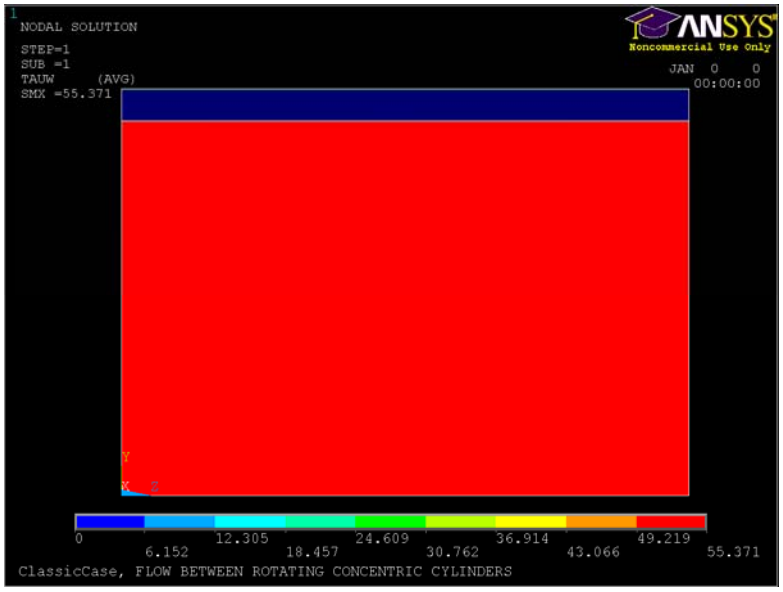

Figure 4.6: Shear Stress on Piston Wall (Classic Case)

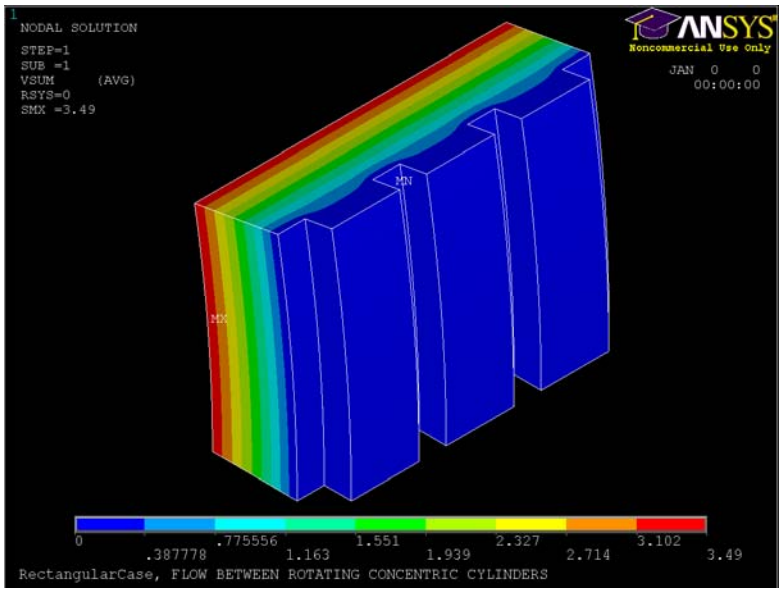

Figure 4.7: Isometric View of Velocity Profile (Non-linear Case)

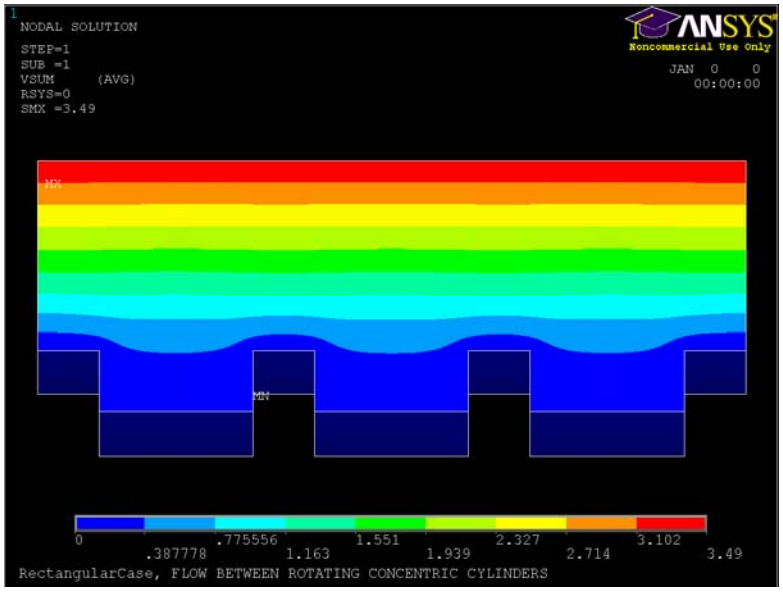

Figure 4.8: Top View of Velocity Profile (Non-linear Case)

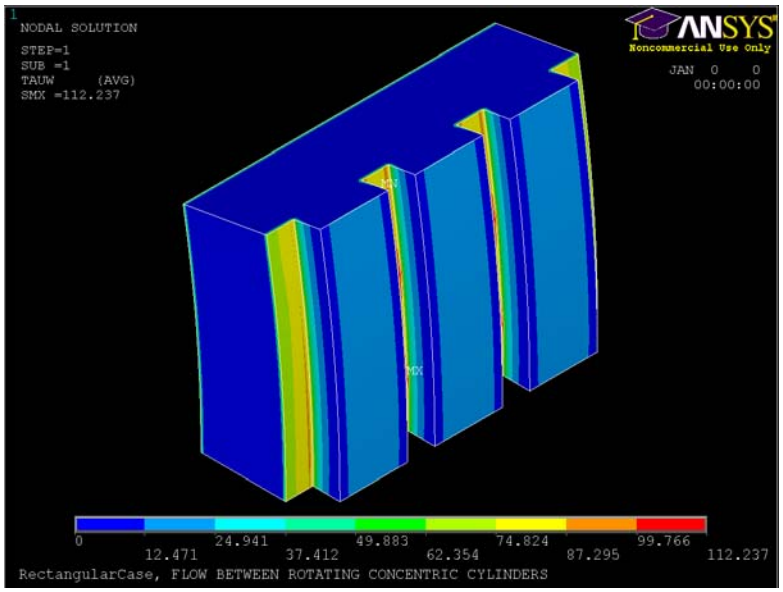

Figure 4.9: Isometric View of Shear Stress Profile (Non-linear Case)

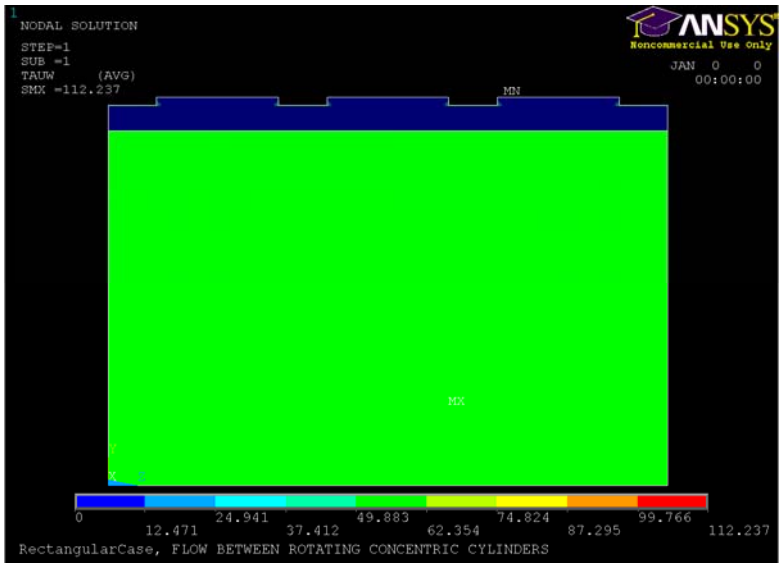

Figure 4.10: Shear Stress Profile on Piston Wall (Non-linear Case)

Chapter 5 CONCLUSIONS

Designing robotic joints with effective variable compliance is an important technology in developing autonomous, safe, and energetically efficient robots. Effective variable compliance may be produced by putting a compliant element such as a spring in parallel with a variable damper such as an MR damper. Effective variable compliance is then achieved through the proper control of this mechanism, which will include switching. Because of this principle many students at OSU's Locomotion and Biomechanics Lab worked to develop linear and rotary MR dampers to be used in robotic transmissions with effective variable compliance. This project studied the effect of adding non-linearities to the inside surface of the cylinder in these dampers in order to increase the magnetic flux density in the fluid gap, while keeping the average fluid gap constant. Such a change was intended to increase the bandwidth of these devices.

This problem was decoupled into a magnetic component and a fluid component. The magnetic component was numerically analyzed in the FEA environment of OctaveFEMM, and the fluid component was analyzed using in the FLOTRAN environment of the computer code ANSYS. Using this setup the magnetic flux density in the gap increased by 21.9%, while the shear stress on the piston wall increased by 10.1%. These results suggest that adding non-linearities to the inside surface of the cylinder while maintaining the same average gap leads to a greater increase in the magnetic flux density in the gap than it does in the shear stress on the piston surface. This fact should allow for the design and development of effective variable compliance robotic transmissions with a greater bandwidth. Such a development in turn will allow for safer and more energetically efficient autonomous robots.

There are further steps that may be taken in improving this analysis. This problem was decoupled into magnetic and fluid components to simplify the analysis; however, by avoiding this decoupling a more accurate study may be possible. Computer programs such as COMSOL allow for the fluid and magnetic components to be analyzed simultaneously, which will avoid the decoupling of this problem. Furthermore, a full analysis of the effect of non-linearities on the performance of this device must include an experimental component to compare the classic MR damper to the non-linear version. In addition, instead of rectangular non-linearities other studies could add semi-circular, triangular, or trapezoidal non-linearities as well. Finally, the effect of damper size on the behavior of the damper may be analyzed by designing multiple classic and non-linear MR dampers with varying overall dimensions but constant relative dimensions. This future work will be important in more conclusively determining the effect of non-linearities on the behavior of MR dampers.

Chapter 6 APPENDIX A

OctaveFEMM Classic Case Code

```
%Smart Materials and Structures Laboratory
%Magneto-Rheological Damper side view (default)
%
%January 19, 2009
%
%Ehsan Sadeghipour
%Dr. Marcelo Dapino

clear all; clc; close all;

inches_to_meters = 0.0254;
air_sphere_radius = 5*inches_to_meters;
cylinder_length = 2.415*inches_to_meters;
cylinder_side_thickness = .375*inches_to_meters;
cylinder_outside_radius = 3.361/2*inches_to_meters;
cylinder_inside_radius = 2.986/2*inches_to_meters;
coil_length = (1.08-.36)*inches_to_meters;
coil_radius = 1.33/2*inches_to_meters;
coil_outside_limit = 2/2*inches_to_meters;
coil_turns = 1210;
coil_current = 1;
axle_sleve_length = .475*inches_to_meters;
axle_sleve_radius = 1/2*inches_to_meters;
axle_length = 8.5*inches_to_meters;
axle_radius = .625/2*inches_to_meters;
piston_thickness = .36*inches_to_meters;
piston_radius = 2.75/2*inches_to_meters;
blocklabel_tolerance = .001;
data_acquisition_tolerance = .005;
inside_cylinder_tolerance = .05;
arc_tolerance = 2.5;
mesh_tolerance = .01;
minimum_mesh_angle = 30;

openfemm;

newdocument(0);

mi_probdef(60, 'meters', 'axi', 1e-15, 0, minimum_mesh_angle);

mi_drawarc([0 -air_sphere_radius; 0 air_sphere_radius], 180, arc_tolerance);
mi_addblocklabel(blocklabel_tolerance, air_sphere_radius -
blocklabel_tolerance);
```

```
mi_drawrectangle(cylinder_inside_radius, -cylinder_length/2,
cylinder_outside_radius, cylinder_length/2);
mi_addblocklabel(cylinder_outside_radius - blocklabel_tolerance,
cylinder_length/2 - blocklabel_tolerance);

mi_drawrectangle(0, cylinder_length/2, cylinder_outside_radius,
cylinder_length/2 + cylinder_side_thickness);
mi_addblocklabel(cylinder_outside_radius - blocklabel_tolerance,
cylinder_length/2 + cylinder_side_thickness - blocklabel_tolerance);

mi_drawrectangle(0, -cylinder_length/2, cylinder_outside_radius, -
cylinder_length/2 - cylinder_side_thickness);
mi_addblocklabel(cylinder_outside_radius - blocklabel_tolerance, -
cylinder_length/2 - cylinder_side_thickness + blocklabel_tolerance);

mi_drawrectangle(0, coil_length/2 + piston_thickness, axle_sleve_radius,
cylinder_length/2);
mi_addblocklabel(axle_radius + blocklabel_tolerance, coil_length/2 +
piston_thickness + blocklabel_tolerance);

mi_drawrectangle(0, -axle_length/2, axle_radius, axle_length/2);
mi_addblocklabel(axle_radius - blocklabel_tolerance, axle_length/2 -
blocklabel_tolerance);

mi_drawrectangle(0, -coil_length/2, coil_radius, coil_length/2);
mi_addblocklabel(coil_radius - blocklabel_tolerance, coil_length/2 -
blocklabel_tolerance);

mi_drawrectangle(0, -coil_length/2-piston_thickness, piston_radius, -
coil_length/2);
mi_addblocklabel(coil_radius - blocklabel_tolerance, -coil_length/2 -
blocklabel_tolerance);

mi_drawrectangle(0, coil_length/2, piston_radius,
coil_length/2+piston_thickness);
mi_addblocklabel(coil_radius - blocklabel_tolerance, coil_length/2 +
blocklabel_tolerance);

mi_drawrectangle(cylinder_inside_radius, -coil_length/2-piston_thickness,
piston_radius, -coil_length/2);
mi_addblocklabel(piston_radius + blocklabel_tolerance, -coil_length/2 -
blocklabel_tolerance);

mi_drawrectangle(cylinder_inside_radius, coil_length/2, piston_radius,
coil_length/2+piston_thickness);
mi_addblocklabel(piston_radius + blocklabel_tolerance, coil_length/2 +
blocklabel_tolerance);

mi_drawrectangle(0, -coil_length/2, coil_outside_limit, coil_length/2);
mi_addblocklabel(coil_outside_limit - blocklabel_tolerance, coil_length/2 -
blocklabel_tolerance);
```

```
mi_addblocklabel(cylinder_inside_radius - blocklabel_tolerance,
cylinder_length/2 - blocklabel_tolerance);
mi_addblocklabel(cylinder_inside_radius - blocklabel_tolerance, coil_length/2
- blocklabel_tolerance);
mi_addblocklabel(cylinder_inside_radius - blocklabel_tolerance, -
coil_length/2 - piston_thickness - blocklabel_tolerance);

mi_selectsegment(axle_radius/2, coil_length/2);
mi_selectsegment(axle_radius/2, -coil_length/2);
mi_selectsegment(axle_radius/2, coil_length/2+piston_thickness);
mi_selectsegment(axle_radius/2, -coil_length/2-piston_thickness);
mi_selectsegment(axle_radius/2, cylinder_length/2);
mi_selectsegment(axle_radius/2, -cylinder_length/2);
mi_selectsegment(axle_radius/2, cylinder_length/2+cylinder_side_thickness);
mi_selectsegment(axle_radius/2, -cylinder_length/2-cylinder_side_thickness);
mi_selectnode(0, coil_length/2);
mi_selectnode(0, -coil_length/2);
mi_selectnode(0, coil_length/2+piston_thickness);
mi_selectnode(0, -coil_length/2-piston_thickness);
mi_selectnode(0, cylinder_length/2);
mi_selectnode(0, -cylinder_length/2);
mi_selectnode(0, cylinder_length/2+cylinder_side_thickness);
mi_selectnode(0, -cylinder_length/2-cylinder_side_thickness);
mi_deleteselected;

mi_addsegment([0 -air_sphere_radius; 0 air_sphere_radius]);

% Define an "asymptotic boundary condition" property.  This will mimic
% an "open" solution domain

%muo = pi*4e-7;

mi_addboundprop('Asymptotic', 0, 0, 0, 0, 0, 0, 0, 0, 0);

mi_addcircprop('coil', coil_current, 1);

% Apply the "Asymptotic" boundary condition to the arc defining the
% boundary of the solution region

mi_selectarcsegment(air_sphere_radius,0);
mi_setarcsegmentprop(2.5, 'Asymptotic', 0, 0);
mi_clearselected

mi_addmaterial('Air', 1, 1, 0, 0, 0, 0, 0, 1, 0, 0, 0);
mi_addmaterial('MR_Fluid', 3.5, 3.5, 0, 0, 0, 0, 0, 1, 0, 0, 0);
mi_addmaterial('Steel', 2000, 2000, 0, 0, 0, 0, 0, 1, 0, 0, 0);
mi_addmaterial('Copper', 1, 1, 0, 0, 0, 0, 0, 0, 3, 1, 0, 0, .001);
mi_addmaterial('Aluminum', 1, 1, 0, 0, 0, 0, 0, 0, 3, 1, 0, 0, .001);

mi_selectlabel(blocklabel_tolerance, air_sphere_radius -
blocklabel_tolerance);
mi_setblockprop('Air', 0, mesh_tolerance, '<None>', 0, 0, 0);
mi_clearselected
```

```
mi_selectlabel(cylinder_inside_radius - blocklabel_tolerance,
cylinder_length/2 - blocklabel_tolerance);
mi_setblockprop('Air', 0, mesh_tolerance, '<None>', 0, 0, 0);
mi_clearselected

mi_selectlabel(cylinder_inside_radius - blocklabel_tolerance, coil_length/2 -
blocklabel_tolerance);
mi_setblockprop('Air', 0, mesh_tolerance, '<None>', 0, 0, 0);
mi_clearselected

mi_selectlabel(cylinder_inside_radius - blocklabel_tolerance, -coil_length/2
- piston_thickness - blocklabel_tolerance);
mi_setblockprop('Air', 0, mesh_tolerance, '<None>', 0, 0, 0);
mi_clearselected

mi_selectlabel(piston_radius + blocklabel_tolerance, -coil_length/2 -
blocklabel_tolerance);
mi_setblockprop('MR_Fluid', 0, mesh_tolerance/10, '<None>', 0, 0, 0);
mi_clearselected;

mi_selectlabel(piston_radius + blocklabel_tolerance, coil_length/2 +
blocklabel_tolerance);
mi_setblockprop('MR_Fluid', 0, mesh_tolerance/10, '<None>', 0, 0, 0);
mi_clearselected;

mi_selectlabel(coil_outside_limit - blocklabel_tolerance, coil_length/2 -
blocklabel_tolerance);
mi_setblockprop('Copper', 0, mesh_tolerance, 'coil', 0, 0, coil_turns);
mi_clearselected;

mi_selectlabel(cylinder_outside_radius - blocklabel_tolerance,
cylinder_length/2 - blocklabel_tolerance);
mi_setblockprop('Steel', 0, mesh_tolerance, '<None>', 0, 0, 0);
mi_clearselected

mi_selectlabel(cylinder_outside_radius - blocklabel_tolerance,
cylinder_length/2 + cylinder_side_thickness - blocklabel_tolerance);
mi_setblockprop('Aluminum', 0, mesh_tolerance, '<None>', 0, 0, 0);
mi_clearselected;

mi_selectlabel(cylinder_outside_radius - blocklabel_tolerance, -
cylinder_length/2 - cylinder_side_thickness + blocklabel_tolerance);
mi_setblockprop('Aluminum', 0, mesh_tolerance, '<None>', 0, 0, 0);
mi_clearselected

mi_selectlabel(axle_radius + blocklabel_tolerance, coil_length/2 +
piston_thickness + blocklabel_tolerance);
mi_setblockprop('Steel', 0, mesh_tolerance, '<None>', 0, 0, 0);
mi_clearselected;

mi_selectlabel(axle_radius - blocklabel_tolerance, axle_length/2 -
blocklabel_tolerance);
```

```
mi_setblockprop('Aluminum', 0, mesh_tolerance, '<None>', 0, 0, 0);
mi_clearselected

mi_selectlabel(coil_radius - blocklabel_tolerance, coil_length/2 -
blocklabel_tolerance);
mi_setblockprop('Steel', 0, mesh_tolerance, '<None>', 0, 0, 0);
mi_clearselected;

mi_selectlabel(coil_radius - blocklabel_tolerance, -coil_length/2 -
blocklabel_tolerance);
mi_setblockprop('Steel', 0, mesh_tolerance, '<None>', 0, 0, 0);
mi_clearselected

mi_selectlabel(coil_radius - blocklabel_tolerance, coil_length/2 +
blocklabel_tolerance);
mi_setblockprop('Steel', 0, mesh_tolerance, '<None>', 0, 0, 0);
mi_clearselected;

% Now, the finished input geometry can be displayed.

mi_zoomnatural

v=ver;
mi_saveas([cd,'/ClassicCase.fem']);

% Now,analyze the problem and load the solution when the analysis is finished

mi_analyze
mi_loadsolution

y1_i = linspace(coil_length/2,coil_length/2+piston_thickness, 50);
y2_i = linspace(-coil_length/2-piston_thickness,-coil_length/2, 50);

x_i = linspace(piston_radius,cylinder_inside_radius);

b1 = zeros(length(x_i), length(y1_i));
b2 = zeros(length(x_i), length(y2_i));
x = zeros(length(x_i), length(y2_i));
y1 = zeros(length(x_i), length(y2_i));
y2 = zeros(length(x_i), length(y2_i));

for i = 1:length(x_i)
    for j = 1:length(y1_i)
        b = mo_getb(x_i(i), y1_i(j));
        b1(i,j) = sqrt(b(1).^2+b(2).^2);
        x(i,j) = x_i(i);
        y1(i,j) = y1_i(j);
    end

    for k = 1:length(y2_i)
        b = mo_getb(x_i(i), y2_i(k));
        b2(i,k) = sqrt(b(1).^2+b(2).^2);
```

```
        y2(i,k) = y2_i(k);
    end
end

b1_mean = mean(mean(b1));
b2_mean = mean(mean(b2));

%The following are material properties for DS7012 from Lord Corp
BH_B = [0 .5 1 1.5];
BH_H = [0 65 200 500];
TH_T = [3 10 20 30 40 50 57 59]*1000;
TH_H = [2 20 40 60 90 125 175 195];
H = polyval(polyfit(BH_B, BH_H, 2), (b1_mean+b2_mean)/2);
tau_y = sqrt(polyval(polyfit(TH_H, TH_T.^2, 1), H));
mu = 0.28;

figure
contour(x, y1, b1); colorbar
print -dpng Figure1

figure
contour(x(.05*length(x_i):.95*length(x_i),.05*length(y1_i):.95*length(y1_i)),
...
    y1(.05*length(x_i):.95*length(x_i),.05*length(y1_i):.95*length(y1_i)),
...
    b1(.05*length(x_i):.95*length(x_i),.05*length(y1_i):.95*length(y1_i)));
colorbar;
print -dpng Figure2

figure
contour(x, y2, b2); colorbar
print -dpng Figure3

figure
contour(x(.05*length(x_i):.95*length(x_i),.05*length(y2_i):.95*length(y2_i)),
...
    y2(.05*length(x_i):.95*length(x_i),.05*length(y2_i):.95*length(y2_i)),
...
    b2(.05*length(x_i):.95*length(x_i),.05*length(y2_i):.95*length(y2_i)));
colorbar;
print -dpng Figure4
```

OctaveFEMM Rectangular Cutouts Code

```
%Smart Materials and Structures Laboratory
%Magneto-Rheological Damper side view (rectangular fins)
%
%February 5, 2009
%
%Ehsan Sadeghipour
%Dr. Marcelo Dapino

clear all; clc; close all;

inches_to_meters = 0.0254;
air_sphere_radius = 5*inches_to_meters;
cylinder_length = 2.415*inches_to_meters;
cylinder_side_thickness = .375*inches_to_meters;
cylinder_outside_radius = 3.361/2*inches_to_meters;
coil_length = (1.08-.36)*inches_to_meters;
coil_radius = 1.33/2*inches_to_meters;
coil_outside_limit = 2/2*inches_to_meters;
coil_turns = 1210;
coil_current = 1;
axle_sleve_length = .475*inches_to_meters;
axle_sleve_radius = 1/2*inches_to_meters;
axle_length = 8.5*inches_to_meters;
axle_radius = .625/2*inches_to_meters;
piston_thickness = .36*inches_to_meters;
piston_radius = 2.75/2*inches_to_meters;
fin_width = .03*inches_to_meters;
fin_gap = (piston_thickness - 4*fin_width)/3;
fin_extension = .000533;
cylinder_inside_radius =
2.986/2*inches_to_meters+4*fin_extension*fin_width/3/fin_gap;
fin_height = fin_extension+4*fin_extension*fin_width/3/fin_gap;
blocklabel_tolerance = .0001;
data_acquisition_tolerance = .005;
inside_cylinder_tolerance = .01;
arc_tolerance = 2.5;
mesh_tolerance = .05;
minimum_mesh_angle = 30;

openfemm;

newdocument(0);

mi_probdef(0, 'meters', 'axi', 1.e-15, 0, minimum_mesh_angle);

mi_drawarc([0 -air_sphere_radius; 0 air_sphere_radius], 180, arc_tolerance);
mi_addblocklabel(blocklabel_tolerance, air_sphere_radius -
blocklabel_tolerance);
```

```
mi_drawrectangle(cylinder_inside_radius, -cylinder_length/2,
cylinder_outside_radius, cylinder_length/2);
mi_addblocklabel(cylinder_outside_radius - blocklabel_tolerance,
cylinder_length/2 - blocklabel_tolerance);

mi_drawrectangle(0, cylinder_length/2, cylinder_outside_radius,
cylinder_length/2 + cylinder_side_thickness);
mi_addblocklabel(cylinder_outside_radius - blocklabel_tolerance,
cylinder_length/2 + cylinder_side_thickness - blocklabel_tolerance);

mi_drawrectangle(0, -cylinder_length/2, cylinder_outside_radius, -
cylinder_length/2 - cylinder_side_thickness);
mi_addblocklabel(cylinder_outside_radius - blocklabel_tolerance, -
cylinder_length/2 - cylinder_side_thickness + blocklabel_tolerance);

mi_drawrectangle(0, coil_length/2 + piston_thickness, axle_sleve_radius,
cylinder_length/2);
mi_addblocklabel(axle_radius + blocklabel_tolerance, coil_length/2 +
piston_thickness + blocklabel_tolerance);

mi_drawrectangle(0, -axle_length/2, axle_radius, axle_length/2);
mi_addblocklabel(axle_radius - blocklabel_tolerance, axle_length/2 -
blocklabel_tolerance);

mi_drawrectangle(0, -coil_length/2, coil_radius, coil_length/2);
mi_addblocklabel(coil_radius - blocklabel_tolerance, coil_length/2 -
blocklabel_tolerance);

mi_drawrectangle(0, -coil_length/2-piston_thickness, piston_radius, -
coil_length/2);
mi_addblocklabel(coil_radius - blocklabel_tolerance, -coil_length/2 -
blocklabel_tolerance);

mi_drawrectangle(0, coil_length/2, piston_radius,
coil_length/2+piston_thickness);
mi_addblocklabel(coil_radius - blocklabel_tolerance, coil_length/2 +
blocklabel_tolerance);

mi_drawrectangle(cylinder_inside_radius, -coil_length/2-piston_thickness,
piston_radius, -coil_length/2);
mi_addblocklabel(piston_radius + blocklabel_tolerance, -coil_length/2 -
blocklabel_tolerance);

mi_drawrectangle(cylinder_inside_radius, coil_length/2, piston_radius,
coil_length/2+piston_thickness);
mi_addblocklabel(piston_radius + blocklabel_tolerance, coil_length/2 +
blocklabel_tolerance);

mi_drawrectangle(0, -coil_length/2, coil_outside_limit, coil_length/2);
mi_addblocklabel(coil_outside_limit - blocklabel_tolerance, coil_length/2 -
blocklabel_tolerance);
```

```
mi_drawrectangle(cylinder_inside_radius, coil_length/2,
cylinder_inside_radius-fin_height, coil_length/2+fin_width);
mi_drawrectangle(cylinder_inside_radius, coil_length/2+fin_width+fin_gap,
cylinder_inside_radius-fin_height, coil_length/2+2*fin_width+fin_gap);
mi_drawrectangle(cylinder_inside_radius, coil_length/2+2*fin_width+2*fin_gap,
cylinder_inside_radius-fin_height, coil_length/2+3*fin_width+2*fin_gap);
mi_drawrectangle(cylinder_inside_radius, coil_length/2+3*fin_width+3*fin_gap,
cylinder_inside_radius-fin_height, coil_length/2+4*fin_width+3*fin_gap);

mi_drawrectangle(cylinder_inside_radius, -coil_length/2,
cylinder_inside_radius-fin_height, -coil_length/2-fin_width);
mi_drawrectangle(cylinder_inside_radius, -coil_length/2-fin_width-fin_gap,
cylinder_inside_radius-fin_height, -coil_length/2-2*fin_width-fin_gap);
mi_drawrectangle(cylinder_inside_radius, -coil_length/2-2*fin_width-
2*fin_gap, cylinder_inside_radius-fin_height, -coil_length/2-3*fin_width-
2*fin_gap);
mi_drawrectangle(cylinder_inside_radius, -coil_length/2-3*fin_width-
3*fin_gap, cylinder_inside_radius-fin_height, -coil_length/2-4*fin_width-
3*fin_gap);

mi_addblocklabel(cylinder_inside_radius - blocklabel_tolerance,
cylinder_length/2 - blocklabel_tolerance);
mi_addblocklabel(cylinder_inside_radius - blocklabel_tolerance, coil_length/2
- blocklabel_tolerance);
mi_addblocklabel(cylinder_inside_radius - blocklabel_tolerance, -
coil_length/2 - piston_thickness - blocklabel_tolerance);

mi_selectsegment(axle_radius/2, coil_length/2);
mi_selectsegment(axle_radius/2, -coil_length/2);
mi_selectsegment(axle_radius/2, coil_length/2+piston_thickness);
mi_selectsegment(axle_radius/2, -coil_length/2-piston_thickness);
mi_selectsegment(axle_radius/2, cylinder_length/2);
mi_selectsegment(axle_radius/2, -cylinder_length/2);
mi_selectsegment(axle_radius/2, cylinder_length/2+cylinder_side_thickness);
mi_selectsegment(axle_radius/2, -cylinder_length/2-cylinder_side_thickness);

mi_selectsegment(cylinder_inside_radius, coil_length/2+fin_width/2);
mi_selectsegment(cylinder_inside_radius,
coil_length/2+fin_width/2+fin_gap+fin_width);
mi_selectsegment(cylinder_inside_radius,
coil_length/2+fin_width/2+2*fin_gap+2*fin_width);
mi_selectsegment(cylinder_inside_radius,
coil_length/2+fin_width/2+3*fin_gap+3*fin_width);

mi_selectsegment(cylinder_inside_radius, -coil_length/2-fin_width/2);
mi_selectsegment(cylinder_inside_radius, -coil_length/2-fin_width/2-fin_gap-
fin_width);
mi_selectsegment(cylinder_inside_radius, -coil_length/2-fin_width/2-
2*fin_gap-2*fin_width);
mi_selectsegment(cylinder_inside_radius, -coil_length/2-fin_width/2-
3*fin_gap-3*fin_width);

mi_selectnode(0, coil_length/2);
mi_selectnode(0, -coil_length/2);
```

```
mi_selectnode(0, coil_length/2+piston_thickness);
mi_selectnode(0, -coil_length/2-piston_thickness);
mi_selectnode(0, cylinder_length/2);
mi_selectnode(0, -cylinder_length/2);
mi_selectnode(0, cylinder_length/2+cylinder_side_thickness);
mi_selectnode(0, -cylinder_length/2-cylinder_side_thickness);
mi_deleteselected;

mi_addsegment([0 -air_sphere_radius; 0 air_sphere_radius]);

% Define an "asymptotic boundary condition" property.  This will mimic
% an "open" solution domain

muo = pi*4e-7;

mi_addboundprop('Asymptotic', 0, 0, 0, 0, 0, 0, 0, 0, 0);

mi_addcircprop('coil', coil_current, 1);

% Apply the "Asymptotic" boundary condition to the arc defining the
% boundary of the solution region

mi_selectarcsegment(air_sphere_radius,0);
mi_setarcsegmentprop(2.5, 'Asymptotic', 0, 0);
mi_clearselected

mi_addmaterial('Air', 1, 1, 0, 0, 0, 0, 0, 0, 0, 0, 0);
mi_addmaterial('MR_Fluid', 3.5, 3.5, 0, 0, 0, 0, 0, 0, 0, 0, 0);
mi_addmaterial('Steel', 2000, 2000, 0, 0, 10.44, 0, 0, 0, 0, 0, 0);
mi_addmaterial('Copper', 1, 1, 0, 0, 59.6, 0, 0, 0, 0, 0, 0, 1, .0040386);
mi_addmaterial('Aluminum', 1, 1, 0, 0, 35.38, 0, 0, 0, 0, 0, 0, 0, 0);

mi_selectlabel(blocklabel_tolerance, air_sphere_radius -
blocklabel_tolerance);
mi_setblockprop('Air', 0, mesh_tolerance, '<None>', 0, 0, 0);
mi_clearselected

mi_selectlabel(cylinder_inside_radius - blocklabel_tolerance,
cylinder_length/2 - blocklabel_tolerance);
mi_setblockprop('Air', 0, mesh_tolerance, '<None>', 0, 0, 0);
mi_clearselected

mi_selectlabel(cylinder_inside_radius - blocklabel_tolerance, coil_length/2 -
blocklabel_tolerance);
mi_setblockprop('Air', 0, mesh_tolerance, '<None>', 0, 0, 0);
mi_clearselected

mi_selectlabel(cylinder_inside_radius - blocklabel_tolerance, -coil_length/2
- piston_thickness - blocklabel_tolerance);
mi_setblockprop('Air', 0, mesh_tolerance, '<None>', 0, 0, 0);
mi_clearselected
```

```
mi_selectlabel(piston_radius + blocklabel_tolerance, -coil_length/2 -
blocklabel_tolerance);
mi_setblockprop('MR_Fluid', 0, mesh_tolerance/10, '<None>', 0, 0, 0);
mi_clearselected;

mi_selectlabel(piston_radius + blocklabel_tolerance, coil_length/2 +
blocklabel_tolerance);
mi_setblockprop('MR_Fluid', 0, mesh_tolerance/10, '<None>', 0, 0, 0);
mi_clearselected;

mi_selectlabel(coil_outside_limit - blocklabel_tolerance, coil_length/2 -
blocklabel_tolerance);
mi_setblockprop('Copper', 0, mesh_tolerance, 'coil', 0, 0, coil_turns);
mi_clearselected;

mi_selectlabel(cylinder_outside_radius - blocklabel_tolerance,
cylinder_length/2 - blocklabel_tolerance);
mi_setblockprop('Steel', 0, mesh_tolerance, '<None>', 0, 0, 0);
mi_clearselected

mi_selectlabel(cylinder_outside_radius - blocklabel_tolerance,
cylinder_length/2 + cylinder_side_thickness - blocklabel_tolerance);
mi_setblockprop('Aluminum', 0, mesh_tolerance, '<None>', 0, 0, 0);
mi_clearselected;

mi_selectlabel(cylinder_outside_radius - blocklabel_tolerance, -
cylinder_length/2 - cylinder_side_thickness + blocklabel_tolerance);
mi_setblockprop('Aluminum', 0, mesh_tolerance, '<None>', 0, 0, 0);
mi_clearselected

mi_selectlabel(axle_radius + blocklabel_tolerance, coil_length/2 +
piston_thickness + blocklabel_tolerance);
mi_setblockprop('Steel', 0, mesh_tolerance, '<None>', 0, 0, 0);
mi_clearselected;

mi_selectlabel(axle_radius - blocklabel_tolerance, axle_length/2 -
blocklabel_tolerance);
mi_setblockprop('Aluminum', 0, mesh_tolerance, '<None>', 0, 0, 0);
mi_clearselected

mi_selectlabel(coil_radius - blocklabel_tolerance, coil_length/2 -
blocklabel_tolerance);
mi_setblockprop('Steel', 0, mesh_tolerance, '<None>', 0, 0, 0);
mi_clearselected;

mi_selectlabel(coil_radius - blocklabel_tolerance, -coil_length/2 -
blocklabel_tolerance);
mi_setblockprop('Steel', 0, mesh_tolerance, '<None>', 0, 0, 0);
mi_clearselected

mi_selectlabel(coil_radius - blocklabel_tolerance, coil_length/2 +
blocklabel_tolerance);
mi_setblockprop('Steel', 0, mesh_tolerance, '<None>', 0, 0, 0);
```

```
mi_clearselected;

% Now, the finished input geometry can be displayed.

mi_zoomnatural

v=ver;
mi_saveas([cd,'/RectangularCase.fem']);

% Now,analyze the problem and load the solution when the analysis is finished

mi_analyze
mi_loadsolution

y1_i = linspace(coil_length/2,coil_length/2+piston_thickness);
y2_i = linspace(-coil_length/2-piston_thickness,-coil_length/2);

x_i = linspace(piston_radius,cylinder_inside_radius-fin_height);

b1 = zeros(length(x_i), length(y1_i));
b2 = zeros(length(x_i), length(y2_i));
x = zeros(length(x_i), length(y2_i));
y1 = zeros(length(x_i), length(y2_i));
y2 = zeros(length(x_i), length(y2_i));

for i = 1:length(x_i)
    for j = 1:length(y1_i)
        b = mo_getb(x_i(i), y1_i(j));
        b1(i,j) = sqrt(b(1).^2+b(2).^2);
        x(i,j) = x_i(i);
        y1(i,j) = y1_i(j);
    end

    for k = 1:length(y2_i)
        b = mo_getb(x_i(i), y2_i(k));
        b2(i,k) = sqrt(b(1).^2+b(2).^2);
        y2(i,k) = y2_i(k);
    end
end

b1_mean = mean(mean(b1));
b2_mean = mean(mean(b2));

%The following are material properties for DS7012 from Lord Corp
BH_B = [0 .5 1 1.5];
BH_H = [0 65 200 500];
TH_T = [3 10 20 30 40 50 57 59]*1000;
TH_H = [2 20 40 60 90 125 175 195];
H = polyval(polyfit(BH_B, BH_H, 2), (b1_mean+b2_mean)/2);
tau_y = sqrt(polyval(polyfit(TH_H, TH_T.^2, 1), H));
mu = 0.28;
```

```
figure
contour(x, y1, b1); colorbar
print -dpng Figure1

figure
contour(x(.05*length(x_i):.95*length(x_i),.05*length(y1_i):.95*length(y1_i)),
...
    y1(.05*length(x_i):.95*length(x_i),.05*length(y1_i):.95*length(y1_i)),
...
    b1(.05*length(x_i):.95*length(x_i),.05*length(y1_i):.95*length(y1_i)));
colorbar;
print -dpng Figure2

figure
contour(x, y2, b2); colorbar
print -dpng Figure3

figure
contour(x(.05*length(x_i):.95*length(x_i),.05*length(y2_i):.95*length(y2_i)),
...
    y2(.05*length(x_i):.95*length(x_i),.05*length(y2_i):.95*length(y2_i)),
...
    b2(.05*length(x_i):.95*length(x_i),.05*length(y2_i):.95*length(y2_i)));
colorbar;
print -dpng Figure4
```

Chapter 7 APPENDIX B

ANSYS Classic Case Code

```
!Smart Materials and Structures Laboratory
!MR Damper - Classic Case
!
!April 19, 2009
!
!Ehsan Sadeghipour
!Dr. Marcelo Dapino
!
!
/VERIFY,ClassicCase
/TITLE, ClassicCase, FLOW BETWEEN ROTATING CONCENTRIC CYLINDERS
!
! -- PARAMETERS --
R1    = .0349                          ! RADIUS OF INNER CYLINDER
R2    = .0379                          ! RADIUS OF OUTER CYLINDER
NX    = 30                             ! NUMBER OF X DIVISIONS
THETA = 10                             ! CYLINDER ENDING ANGLE
NY    =  10                            ! NUMBER OF Y DIVISIONS
LZ    = .0092                          ! LENGTH IN Z DIRECTION
NZ    =  92                            ! NUMBER OF Z DIVISIONS
OMEGA = 100                            ! ANGULAR VELOCITY
RHO   = 2380                           ! FLUID DENSITY
MU    = .042                           ! FLUID VISCOSITY
! -- MODEL --
/PREP7
smrt,off
ET,1,FLUID142,,,3                      ! 3D RTZ SYSTEM
MSHK,1                                 ! MAPPED VOLUME MESH
MSHA,0,3D                              ! USING HEX

CYLIND,R1,R2,,LZ,,THETA
LSEL,S,,,1,8,7
LSEL,A,,,3,6,3
LESIZE,ALL,,,NX
LSEL,S,,,2,7,5
LSEL,A,,,4,5
LESIZE,ALL,,,NY
LSEL,S,,,9,12
LESIZE,ALL,,,NZ
ALLSEL
VMESH,1

ASEL,S,,,4                             ! INNER CYLINDER BOUNDARY CONDITIONS
NSLA,S,1
D,ALL,VX
```

```
D,ALL,VY,-R1*OMEGA
D,ALL,VZ
D,ALL,PRES
D,ALL,ENKE,-1

ASEL,S,,,3                              ! OUTER CYLINDER BOUNDARY CONDITIONS
NSLA,S,1
D,ALL,VX
D,ALL,VY
D,ALL,VZ

ASEL,S,,,5                              ! PERIODIC BOUNDARY CONDITIONS
NSLA,S,1
D,ALL,VX
D,ALL,VX
PERI,,THETA                             ! PERIODIC BC MACRO

ASEL,S,,,1,2                            ! SYMMETRY BOUNDARY CONDITIONS
NSLA,S,1
D,ALL,VX
D,ALL,VZ

ALLSEL
FINISH
! -- SOLUTION --
/SOLU
FLDATA,ITER,EXEC,5000                   ! NUMBER OF GLOBAL ITERATIONS
FLDATA,NOMI,DENS,RHO                    ! NOMINAL DENSITY
FLDATA,NOMI,VISC,MU                     ! NOMINAL VISCOSITY
FLDATA,OUTP,TAUW,T                      ! OUTPUT WALL SHEAR STRESS
CGOMGA,,,OMEGA                          ! ANGULAR VELOCITY OF ROTATING CS
SAVE
/OUTPUT,SCRATCH                         ! DIVERT OUTPUT
SOLVE
/OUTPUT
FINISH
!
```

ANSYS Rectangular Cutouts Code

```
!Smart Materials and Structures Laboratory
!MR Damper w/ Rectangular Cutouts
!
!April 19, 2009
!
!Ehsan Sadeghipour
!Dr. Marcelo Dapino
!
!
/TITLE, RectangularCase, FLOW BETWEEN ROTATING CONCENTRIC CYLINDERS
```

```
!
! -- PARAMETERS --
R1    = .0349                       ! RADIUS OF INNER CYLINDER
R2    = .0382                       ! RADIUS OF OUTER CYLINDER
FH    = .0008                       ! FIN HEIGHT
FW    = .0008                       ! FIN wIDTH
PT    = .0092                       ! PISTON THICKNESS
GT    = .0020                       ! GAP THICKNESS
XT    = .0001                       ! X THICKNESS
THETA = 10                          ! CYLINDER ENDING ANGLE
YT    =  1                          ! Y THICKNESS
ZT    = .0001                       ! Z THICKNESS
OMEGA = 100                         ! ANGULAR VELOCITY
RHO   = 2380                        ! FLUID DENSITY
MU    = .042                        ! FLUID VISCOSITY
! -- MODEL --
/PREP7
smrt,off
ET,1,FLUID142,,,3                   ! 3D RTZ SYSTEM
MSHK,1                              ! MAPPED VOLUME MESH
MSHA,0,3D                           ! USING HEX


CYLIND,R1,R2,,PT,,THETA             ! CREATING THE VOLUME
CYLIND,R2-FH,R2,,FW,,THETA
CYLIND,R2-FH,R2,FW+GT,2*FW+GT,,THETA
CYLIND,R2-FH,R2,2*FW+2*GT,3*FW+2*GT,,THETA
CYLIND,R2-FH,R2,PT-FW,PT,,THETA
VSBV,1,2,DELETE,DELETE
VSBV,6,3,DELETE,DELETE
VSBV,1,4,DELETE,DELETE
VSBV,2,5,DELETE,DELETE

LSEL,S,,,11,12                      ! Z AXIS DIVISIONS
LSEL,A,,,23,59,12
LSEL,A,,,24,60,12
LSEL,A,,,4,9,5
LSEL,A,,,15,16
LSEL,A,,,21,22
LESIZE,ALL,ZT

LSEL,S,,,61,62                      ! X AXIS DIVISIONS
LSEL,A,,,1,3,2
LSEL,A,,,49,51,2
LSEL,A,,,42,44,2
LSEL,A,,,37,39,2
LSEL,A,,,30,32,2
LSEL,A,,,25,27,2
LSEL,A,,,18,20,2
LESIZE,ALL,XT

LSEL,S,,,2,14,12                    ! Y AXIS DIVISIONS
LSEL,A,,,17,19,2
LSEL,A,,,26,28,2
LSEL,A,,,29,31,2
```

```
LSEL,A,,,38,40,2
LSEL,A,,,41,43,2
LSEL,A,,,50,52,2
LSEL,A,,,7,55,48
LESIZE,ALL,,YT

VSWEEP,1,15,6,1

ASEL,S,,,4                          ! INNER CYLINDER BOUNDARY CONDITIONS
NSLA,S,1
D,ALL,VX
D,ALL,VY,-R1*OMEGA
D,ALL,VZ
D,ALL,PRES
D,ALL,ENKE,-1

ASEL,S,,,10,28,3                    ! OUTER CYLINDER BOUNDARY CONDITIONS
ASEL,A,,,8,20,6
ASEL,A,,,3,5,2
ASEL,A,,,9
NSLA,S,1
D,ALL,VX
D,ALL,VY
D,ALL,VZ

ASEL,S,,,6                          ! PERIODIC BOUNDARY CONDITIONS
NSLA,S,1
D,ALL,VX
D,ALL,VZ
PERI,,THETA                         ! PERIODIC BC MACRO

ASEL,S,,,1,31,30                    ! SYMMETRY BOUNDARY CONDITIONS
NSLA,S,1
D,ALL,VX
D,ALL,VZ

ALLSEL
FINISH

! -- SOLUTION --
/SOLU
FLDATA,ITER,EXEC,5000                ! NUMBER OF GLOBAL ITERATIONS
FLDATA,NOMI,DENS,RHO                 ! NOMINAL DENSITY
FLDATA,NOMI,VISC,MU                  ! NOMINAL VISCOSITY
FLDATA,OUTP,TAUW,T                   ! OUTPUT WALL SHEAR STRESS
CGOMGA,,,OMEGA                       ! ANGULAR VELOCITY OF ROTATING CS
SAVE
/OUTPUT,SCRATCH                      ! DIVERT OUTPUT
SOLVE
/OUTPUT
FINISH
!
```

Chapter 8 LIST OF REFERENCES

Alexander, R. M. (1990). Three Uses for Springs in Legged Locomotion. *International Journal of Robotics Research* , 53-61.

Bicchi, A., & Tonietti, G. (2004). Fast and "Soft-Arm" Tactics. *IEEE Robotics & Automation Magazine* , 22-33.

Bunting, T. (2005). *Design and Testing of a Variable Effective.* Columbus, OH: The Ohio State University.

Dapino, M. (2008). *ME 774: Smart Materials and Intelligent Systems Course Notes.* Columbus, OH: The Ohio State University.

Farjoud, A., Vahdati, N., & Fook Fah, Y. (2008). Mathematical Model of Drum-type MR Brakes using Herschel-Bulkley Shear Model. *Journal of Intelligent Material Systems and Structures* , 565-572.

Honda Motor Co. Ltd. (2007). *ASIMO Technical Information.* Public Relations Division.

McMahon, T. A. (1984). *Muscles, Reflexes, and Locomotion.* Princeton: Princeton University Press.

Sabatka, K. (2006). *Design and Testing of an MR Drum Rotary Device to Achieve a Variable Effective Compliance Transmission.* Columbus, OH: The Ohio State University.

Westervelt, E. R., Schmiedeler, J. P., & Washington, G. (2004). Variable Transmission Compliance with an MR Damper. *Proceedings of the 2004 ASME IMECE.* Anaheim, CA.

White, F. M. (2005). *Viscous Fluid Flow.* New York City: McGraw-Hill Higher Education.

Yang, T., Westervelt, E. R., & Schmiedeler, J. P. (2007). Using Parallel Joint Compliance to Reduce the Cost of Walking in a Planar Bipedal Robot. *Proceedings of the 2007 ASME IMECE.* Seattle, WA.